ACS APPLIED POLYMER MATERIALS

pubs.acs.org/acsapm Article

Tröger's Base-Cored Triarylamine Polyamide for Electrochromic Response Capability Enhancement

Min-Hsiu Tu,[§] Yu-Jen Shao,[§] Hou-Lin Li,[§] Chien-Chieh Hu,* and Guey-Sheng Liou*

Cite This: *ACS Appl. Polym. Mater.* 2024, 6, 658−668 Read Online

ACCESS | Metrics & More | Article Recommendations | Supporting Information

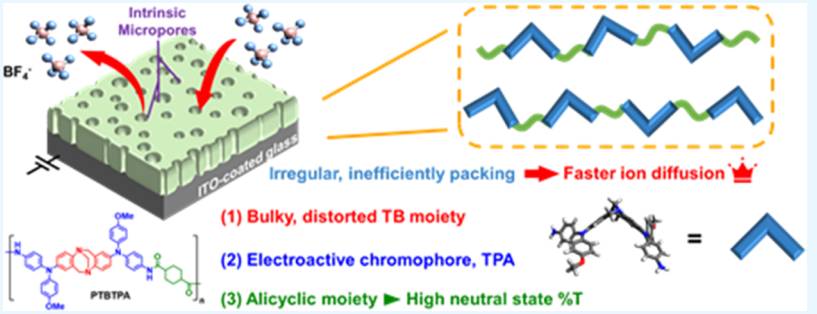

ABSTRACT: Recently, more and more researchers have focused on generating "pores" within the polymer matrix to prompt the performance of electrochromic (EC) films using physical or chemical approaches. In this work, we meticulously designed a Tröger's base (TB)-cored arylamine-containing diamine monomer, TBTPA-NH_2, and synthesized the corresponding redox-active polyamide, PTBTPA. The resulting PTBTPA exhibits low density with large *d*-spacing and surface area, contributing to the rigid and V-shaped TB unit. Consequently, the prepared polymer film demonstrated remarkable electrochemical and EC behaviors, such as low applied potential (1.00 V), facilitating rapid diffusion of the electrolyte, reasonable switching capability (1.8 s/1.5 s for coloring t_c and bleaching t_b, respectively), and excellent stability. For further application, the electrochromic device (ECD) of PTBTPA/HV exhibits the best-enhanced response capability (3.5 s/6.1 s for t_c and t_b, respectively), the highest coloration efficiency (337 cm^2/C), and switching stability (96.1% of retention after 500-cycle switching).

KEYWORDS: *electrochromism, quick response capability, intrinsic microporosity, Tröger's base, triarylamine*

1. INTRODUCTION

With the thriving electronic industry in the past few decades, the development of novel optoelectronic materials has rapidly progressed. Electrochromic (EC) materials have become attractive due to the reversible color change under electrochemical oxidation and reduction.[1−3] With the controllable optical behaviors and energy storage potential, EC materials reveal promising applications in several regions, including transparent displays, antiglare mirrors, smart windows, adaptive camouflage, supercapacitors, and batteries.[4−12] Triphenylamine (TPA) is a representative EC material with high optical contrast between the transparent neutral state and the colored oxidation state. TPA-derived polymers have become spotlights due to their excellent electrochemical and EC characteristics and tunable structures.[13−17] The imperative features of an ideal EC material include a low oxidation voltage, fast response speed, high optical contrast, coloration efficiency, and good long-term stability. The most intuitive approach to increasing the visual contrast for an EC device is thickening the electroactive polymer layer. However, the thicker film would enormously sacrifice the neutral state transparency and simultaneously inhibit the mobility of the counterions, resulting in lower optical contrast and extended response time.[18] To overcome this predicament, our group has demonstrated that making the polymer of intrinsic microporosity (PIM) films by introducing rigid and bulky scaffolds, like iptycene or Tröger's base (TB), is a practical approach to enhance the response capacity of EC devices (ECDs) by generating micropores while keeping high transparency and stiffness of the polymers.[12,19−21]

PIM membranes are polymers containing less than two nm diameter pores, which can be utilized for various purposes, including heterogeneous catalysis, gas separations, and hydrogen storage.[22−26] The general strategy of preparing PIMs is introducing rigid and highly contorted moieties to the polymer backbone, such as ethanoanthracene,[27] iptycene,[28,29] spirobifluorene,[30,31] and Tröger's base.[32,33] The bulky moiety

Received: September 25, 2023
Revised: December 8, 2023
Accepted: December 13, 2023
Published: December 25, 2023

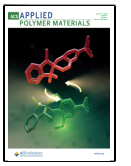

https://doi.org/10.1021/acsapm.3c02288
ACS Appl. Polym. Mater. 2024, 6, 658−668

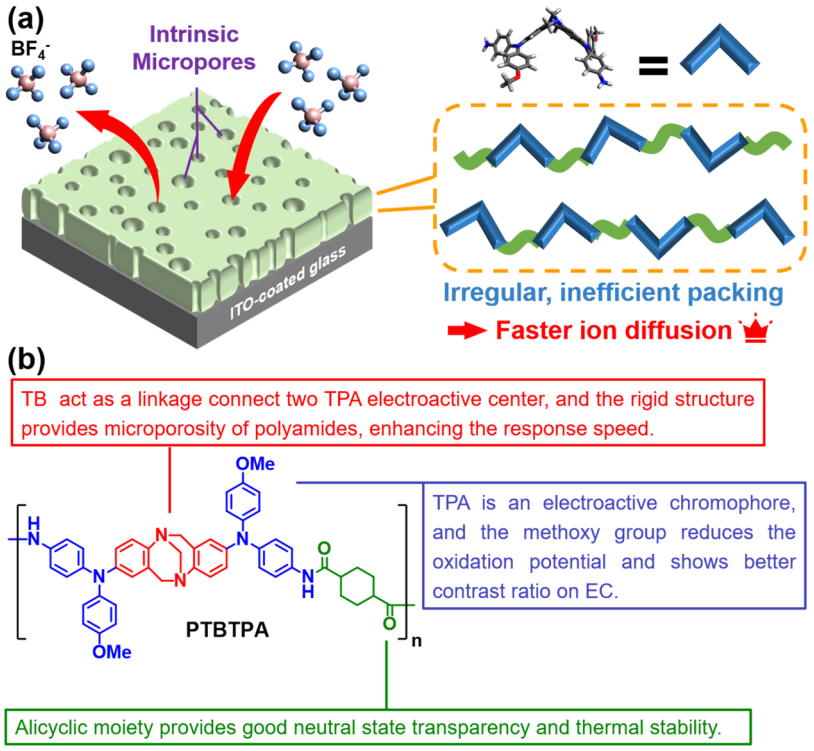

Figure 1. (a) Schematic presentation of the intrinsic microporous polyamide design concept. (b) Design structure of intrinsically porous polyamide, PTBTPA.

Scheme 1. Synthetic Process of (a) TBTPA-NH_2 and (b) Polyamides Was Investigated in This Study[a]

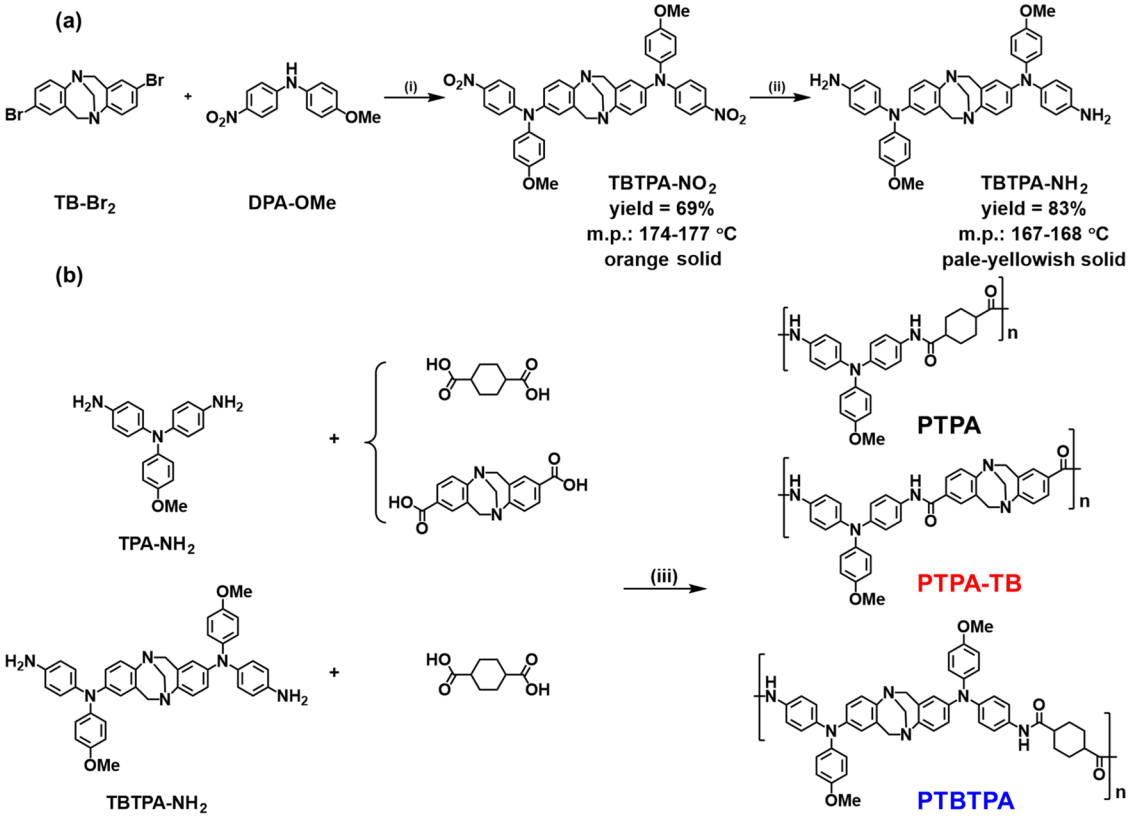

[a](i) Cu, K_2CO_3, and 18-crown-6 ether in *o*-DCB at 160 °C for 2 days; (ii) hydrazine and Pd/C in THF/ethanol at reflux temperature for 2 days; and (iii) TPP, $CaCl_2$, and pyridine in NMP at 110 °C for 4 h.

https://doi.org/10.1021/acsapm.3c02288
ACS Appl. Polym. Mater. 2024, 6, 658−668

effectively prevents the polymer chains from dense packing in the solid state, generating microporous cavities between the chains.[34] TB is a rigid V-shape structure consisting of two aniline moieties connected with methylene bridges, first reported by Tröger in 1887.[35] The highly rigid scaffolds of TB are the features that enhance the thermal stability of materials by increasing Tg and generating intrinsic micropores with the V-shape cavity. In 2013, McKeown's group synthesized a series of TB-containing polymers and investigated their gas separation behaviors.[32] The rigid nonplanar structure increased the microporous characteristics, increasing the permeabilities significantly, and the performance far exceeded Robeson's 2008 upper bounds. Besides the applications in gas separation, the rigid structure and electron-rich scaffold of TB made it an ideal hole-transporting material with high thermal stability and charge mobility.[36−38]

In the previous studies of our group, the TB moieties could be inserted into microporous EC polyamides by replacing the dicarboxylic acid monomers with a TB-containing one. However, as an aromatic diacid, the TB diacid-derived polyamides revealed a light-yellow color at the neutral state compared to those derived from aliphatic diacids. Moreover, being an electron-rich pendent group, we surmised that the TB scaffold could lower the oxidation potential if the TB moiety is directly connected to the electroactive TPA center. Hence, a novel diamine monomer, TBTPA-NH_2, has been designed and synthesized for obtaining the corresponding intrinsic microporous polyamide, PTBTPA (Figure 1). A TB linkage connects two TPA moieties to form a rigid, bulky, and electroactive diamine monomer. Moreover, alicyclic diacids would be a better replacement for aromatic ones, the fixed ring structure avoids the drawbacks of losing good thermal properties, and the aliphatic nature not only increases the transparency of the neutral state but also provides good solubility of polymers for the membrane preparation.[39] Therefore, this microporous EC polyamide approach adopts the TB moiety's advantages, giving a high contrast and fast response redox-active material.

2. EXPERIMENTAL SECTION

2.1. Materials. 2,8-Dibromo-6*H*,12*H*-5,11-methanodibenzo[*b*,*f*][1,5]-diazocine (TB-Br_2),[40] 4-methoxy-4′-nitrodiphenylamine (DPA-OMe),[41] and 4,4′-diamino-4″-methoxytriphenylamine (TPA-NH_2)[13] were synthesized according to the previous studies. Tetrabutylammonium tetrafluoroborate ($TBABF_4$) was synthesized by the following steps: the solution of tetrabutylammonium bromide (TBABr) in DI water was added into the saturated solution of sodium tetrafluoroborate ($NaBF_4$) in DI water under vigorous stirring. Then, the obtained white precipitate was recrystallized with a 2:1 water/ethanol solution. Other materials such as 4-bromoanisole (Alfa), cyclohexane dicarboxylic acid (Acros), triphenyl phosphite (TPP) (Acros), potassium carbonate (Alfa), copper powder (Acros), 18-crown-6 ether (TCI), hydrazine monohydrate (Alfa), palladium on activated charcoal (Pd/C) (Acros), and all of the solvents were commercially available.

2.2. Synthesis of Monomers. *2.2.1. N,N′-bis(4-methoxyphenyl)-N,N′-bis(4-nitrophenyl)-6H,12H-5,11-methanodibenzo [b,f][1,5] diazocine-2,8-diamine (TBTPA-NO_2).* As illustrated in Scheme 1a, TB-Br_2 (3.80 g, 10.00 mmol) and DPA-OMe (5.86 g, 24.00 mmol) were dissolved in 40 mL of 1,2-dichlorobenzene (*o*-DCB) in a 100 mL three-neck flask under a nitrogen atmosphere. Copper powder (1.53 g, 24.00 mmol), potassium carbonate (6.63 g, 48.00 mmol), and 18-crown-6 ether (0.53 g, 2.00 mmol) were then added. The reaction mixture was then heated to 160 °C and stirred for 2 days. When the reaction was completed, the mixture was hot-filtered through Celite to remove the residue of copper powder and salts. After the filtrate was cooled, it was poured into 200 mL of water and extracted with 100 mL of dichloromethane three times. The organic layer was combined, and the solvent was removed by rotary evaporation. The crude product was purified by column chromatography (SiO_2, DCM/EA = 9:1) to give TBTPA-NO_2 as an orange solid (4.86 g, yield = 69%), mp 174−177 °C; ^{1}H NMR (600 MHz, DMSO-d_6, δ): 8.00 (d, J = 9.4 Hz, 4H), 7.19 (d, J = 8.9 Hz, 4H), 7.17 (d, J = 8.6 Hz, 2H), 7.10 (dd, J = 8.6, 2.5 Hz, 2H), 6.99 (d, J = 8.9 Hz, 4H), 6.92 (d, J = 2.5 Hz, 2H), 6.60 (d, J = 9.4 Hz, 4H), 4.58 (d, J = 17.1 Hz, 2H), 4.20 (s, 2H), 4.12 (d, J = 17.1 Hz, 2H), 3.77 (s, 6H). ^{13}C NMR (150 MHz, DMSO-d_6, δ): 157.77, 153.85, 146.08, 140.07, 138.02, 137.29, 129.60, 128.97, 126.54, 125.63, 125.45, 124.83, 115.53, 115.03, 65.74, 57.46, 55.33. HRMS (m/z), [M + H^+] calculated: 707.2613, found: 707.2616.

2.2.2. N,N′-bis(4-aminophenyl)-N,N′-bis(4-methoxylphenyl)-6H,12H-5,11-methanodibenzo [b,f][1,5] diazocine-2,8-diamine (TBTPA-NH_2). As illustrated in Scheme 1a, TBTPA-NO_2 (3.53 g, 5.00 mmol) was dissolved in a mixture of 25 mL of tetrahydrofuran (THF) and 25 mL of ethanol in a 100 mL three-neck flask under a nitrogen atmosphere. The reaction mixture was heated to reflux, and Pd/C (0.35g) was added. Hydrazine monohydrate (7.4 mL, 150 mmol) was then added dropwise. After the reaction mixture was refluxed and stirred for 2 days, the mixture was hot-filtered through Celite to remove Pd/C. The filtrate was collected, and THF was removed by rotary evaporation. After a day of precipitation, TBTPA-NH_2 was given as a pale yellowish solid (2.69 g, 83%), mp 167−168 °C; ^{1}H NMR (600 MHz, DMSO-d_6, δ): 6.87 (d, J = 9.1 Hz, 4H), 6.84 (d, J = 8.8 Hz, 2H), 6.81 (d, J = 9.1 Hz, 4H), 6.72 (d, J = 8.6 Hz, 4H), 6.55 (dd, J = 8.8, 2.6 Hz, 2H), 6.51 (d, J = 8.6 Hz, 4H), 6.29 (d, J = 2.6 Hz, 2H), 4.96 (s, 4H), 4.38 (d, J = 16.8 Hz, 2H), 4.08 (s, 2H), 3.84 (d, J = 16.8 Hz, 2H), 3.70 (s, 6H). ^{13}C NMR (150 MHz, DMSO-d_6, δ): 154.70, 145.57, 144.74, 141.04, 140.56, 135.95, 128.34, 127.38, 125.20, 125.12, 118.47, 116.50, 114.88, 114.58, 66.43, 57.81, 55.15. HRMS (m/z), [M^+] calculated: 646.3056, found: 646.3049.

2.3. Synthesis of Polyamides. *2.3.1. Preparation of PTBTPA.* As illustrated in Scheme 1b, 0.103 g (0.6 mmol) of 1,4-cyclohexane dicarboxylic acid and 49.0 mg of calcium chloride were dissolved in 0.8 mL of *N*-methyl-2-pyrrolidone (NMP) in a 10 mL two-neck flask under a nitrogen atmosphere. TBTPA-NH_2 (0.388 g, 0.6 mmol), pyridine (0.3 mL), and TPP (314 μL, 1.2 mmol) were added, and the mixture was then heated to 110 °C and stirred. After 30 min of stirring, the polymer solution turned sticky, and 0.6 mL of NMP was then added for dilution. The dilution process was repeated two times in the following 1 h. After 1.5 h of the total reaction time, the polymer solution was poured into methanol to form a polymer string. The polymer was then washed by Soxhlet extraction with methanol and water for 2 days, respectively. After drying in a vacuum oven at 100 °C, PTBTPA was given as a pale-brownish string (0.451 g, yield = 96%). The inherent viscosity of PTBTPA was 0.61 dL/g (measured in NMP at 30 °C of the concentration of 0.5 g/dL).

2.3.2. Preparation of Polyamide Films. Two types of polymer films were fabricated for different experiments. A free-standing thick film was made by dissolving 80 mg of polymer in 3 mL of dimethylacetamide (DMAc). The solution was filtrated through a syringe filter and drop-casting on a glass slide of 75 × 26 mm^2, which was placed in a vacuum oven to remove most of the solvent at room temperature. The temperature was then increased to 180 °C for 12 h to dry the film completely. The obtained films were about 20 ± 3 μm thick and were used for solubility tests, thermal analysis, WXRD, and BET measurements.

The polymeric electrode for electrochemical analysis was prepared using a polymer solution with a concentration of 2 mg/mL in DMAc. 600 μL of the polymer solution was drop-cast on an ITO-coated glass with a size of 30 × 25 mm^2. The solvent was removed primarily under vacuum at room temperature and dried at 180 °C for 12 h. The obtained films were about 360 ± 30 nm thick and were cut into 30 × 6 mm^2 pieces for further experiment. The polymeric electrodes were scratched into a 20 × 6 mm^2 coated area for the electrochemical impedance spectroscopy measurements to gain better results.

https://doi.org/10.1021/acsapm.3c02288
ACS Appl. Polym. Mater. 2024, 6, 658−668

2.3.3. Fabrication of the Electrochromic Devices (ECDs). An ECD is made by the following steps. First, two pieces of ITO-coated glass with a size of 25 × 30 mm^2 were prepared as two electrodes, and one of the ITO-coated glass was coated with electroactive polyamides with 360 ± 30 nm in thickness. Second, the thermoset adhesive frame (20 × 20 mm^2) with a 5 mm width break was dispensed via an autodispenser. Then, the two glasses were stuck together to form an empty device. The gap distance was controlled by the 120 μm spacer in the adhesive. The adhesive was cured in an oven at 120 °C for 3 h. Finally, the gel-type electrolyte was injected into the device from the 5 mm width break under vacuum conditions, and the break was sealed with UV gel. The gel-type electrolyte was prepared with 670 mg of PMMA, 165 mg of $TBABF_4$ (0.1 M), 40 mg of HV (0.015 M), and 5 mL of propylene carbonate (PC). The total volume of the injected electrolyte was around 48 μL.

2.3.4. Measurements of Electrochemical and Spectroelectrochemical Properties. Electrochemical property analysis, including cyclic voltammetry (CV), differential pulse voltammetry (DPV), and spectroelectrochemical analysis, was performed with a CHI-6122E electrochemical analyzer (CH Instruments). For the samples of small molecule solution, the experiment was measured with an optically transparent thin-layer electrochemical cell (OTTLE cell) conducted with a three-electrode system consisting of a platinum net (1 cm × 2.5 cm) as the working electrode, a platinum wire as the counter electrode, and Ag/AgCl as the reference electrode. The sample with a certain concentration was prepared in 1 mL of anhydrous γ-butyrolactone with 0.1 M tetrabutylammonium perchlorate (TBAP) as a supporting electrolyte. The solution would be purged with nitrogen gas for 30 min before the preparation and measurement, and the OTTLE cell was kept in a nitrogen atmosphere during the measurement. For the samples of polyamide films, the experiment was measured with a three-electrode system consisting of polymer films coated on 0.6 cm × 3 cm ITO glass as the working electrode, platinum as the counter electrode, and Ag/AgCl as the reference electrode in 3 mL of anhydrous acetonitrile with 0.1 M $TBABF_4$ as the supporting electrolyte. The absorption spectra of spectroelectrochemical analysis were recorded by an Agilent 8453 UV−visible diode array spectrophotometer.

3. RESULTS AND DISCUSSION

3.1. Synthesis and Characterization of the Monomers and Model Compounds. The diamine monomer, *N*,*N*′-bis(4-aminophenyl)-*N*,*N*′-bis(4-methoxyphenyl)-6*H*,12*H*-5,11-methanodibenzo[*b*,*f*][1,5]diazocine-2,8-diamine ($TBTPA\text{-}NH_2$), was synthesized by Ullmann condensation with $TB\text{-}Br_2$ and DPA-OMe for the precursor dinitro compound ($TBTPA\text{-}NO_2$) first, following the Pd/C-catalyzed hydrogenation. The detailed synthetic procedures are described in Scheme 1 and Section 2. The characterization of the monomers and the precursors was carefully investigated with elemental analysis and IR, NMR, and ESI-MS spectroscopies, as illustrated in Figures S1−S10. For $TBTPA\text{-}NO_2$, the characteristic absorption of NO_2 stretching in the IR spectrum appeared at 1589 and 1309 cm^{-1}. After hydrogenation, the characteristic peaks of NO_2 stretching disappeared with the generated NH_2 stretching and bending peaks located at 3442, 3362, and 1611 cm^{-1}, respectively, for $TBTPA\text{-}NH_2$. For the ^1H NMR spectrum of $TBTPA\text{-}NO_2$ and $TBTPA\text{-}NH_2$ in Figures S2 and S5, it is worth noting that the proton signals of methylene bridges (H_i) of TB moieties split into two doublets ($H_{i,\,exo}$, $H_{i,\,endo}$) due to the rigid and unflippable structures. The protons at the endo position faced a more shielding effect from the aromatic rings, resulting in an upfield shift.[40] Compared with the ^1H NMR spectra of $TBTPA\text{-}NO_2$ and $TBTPA\text{-}NH_2$, H_e revealed a large upfield shift from 8.00 to 6.51 ppm, indicating the conversion of electron-withdrawing nitro groups to electron-donating amine groups. Moreover, the peak assignments of the $^1H-^1H$ COSY and $^1H-^{13}C$ HSQC NMR spectra of the dinitro and diamine compounds revealed good agreement with the expected structures.

To clarify the electrochemical behaviors of the derived polymers, the amide-type model compounds, TPA-M and TBTPA-M, were prepared via phosphorylation-based condensation of $TPA\text{-}NH_2$ and $TBTPA\text{-}NH_2$ with cyclohexane dicarboxylic acid, as shown in Scheme S1. The IR spectrum of TBTPA-M showed the characteristic peaks of amide N−H stretching at 3303 cm^{-1} and C═O stretching at 1663 cm^{-1}, indicating the formation of amide linkages. In Figures S11−S16, the peak assignments of the ^1H NMR and ^{13}C NMR spectra of TBTPA-M also agreed with the supposed structures. The ^1H NMR revealed the characteristic peaks of amide protons at 9.68 ppm and the proton signals of cyclohexane at 2.32−1.13 ppm, showing the successful end-capping of cyclohexane-amide.

3.2. Synthesis, Characterization, and Basic Properties of Polyamides. Three polyamides were prepared to study the relationship between the microporosity and EC behaviors, and the synthetic process is depicted in Scheme 1b. First, a classic polyamide (PTPA), polymerized from $TPA\text{-}NH_2$ and 1,4-cyclohexane dicarboxylic acid via phosphorylation polymerization, is used as a control group. In addition, there are two polyamides with distorted TB units in the polymer backbone: one is introduced in the diacid unit, PTPA-TB, and the other is by polymerization with the synthesized diamine in this work, PTBTPA.[20] IR and NMR spectroscopies were utilized to investigate the characterizations of these three polyamides. In Figure S17, PTPA showed the amide N−H stretching at 3308 cm^{-1} and C═O stretching at 1662 cm^{-1}, while the same characteristic peaks of the other polyamides were observed at 3314 and 1665 cm^{-1} (PTBTPA) and 3312, and 1650 cm^{-1} (PTPA-TB). The wavenumber of the C═O stretching peak of PTPA-TB was lower than that of other polyamides due to the resonance effect of aromatic acid. The ^1H NMR spectrum of PTBTPA is recorded in Figure S18, and the assignments match the model compound.

The basic properties and the solubility tests of the polyamides are summarized in Tables S1 and S2. These three polyamides revealed sufficiently high molecular weight (M_n > 42 kDa), which could form flexible and free-standing films (Figure S19, thickness: 30 ± 5 μm) for further measurements. Due to the rigid backbone of the TB scaffolds, the hydrodynamic radius of PTBTPA should be larger than the polystyrene standard, resulting in a higher deviation from the molecular weight.[42]

3.2.1. Thermal Properties of Polyamides. Thermogravimetric analysis (TGA), thermomechanical analysis (TMA), and differential scanning calorimetry (DSC) were employed to evaluate the thermal properties of PTPA, PTBTPA, and PTPA-TB, respectively. The high thermal stability of these three polyamides was demonstrated and is illustrated in Figures S20−S22 and Table S3. The DSC traces of the polyamides revealed the endothermic process of glass transition, showing the glass-transition temperature (T_g) of PTPA at 254 °C and that of PTBTPA at 280 °C, demonstrating that the rigidity of the polymer backbone could be enhanced by introducing the TB unit. However, due to its stiffer backbone, the glassy transition was less discernible in the wholly aromatic polyamide PTPA-TB. Besides, the softening temperatures (T_s) of these polyamides followed the

https://doi.org/10.1021/acsapm.3c02288
ACS Appl. Polym. Mater. 2024, 6, 658−668

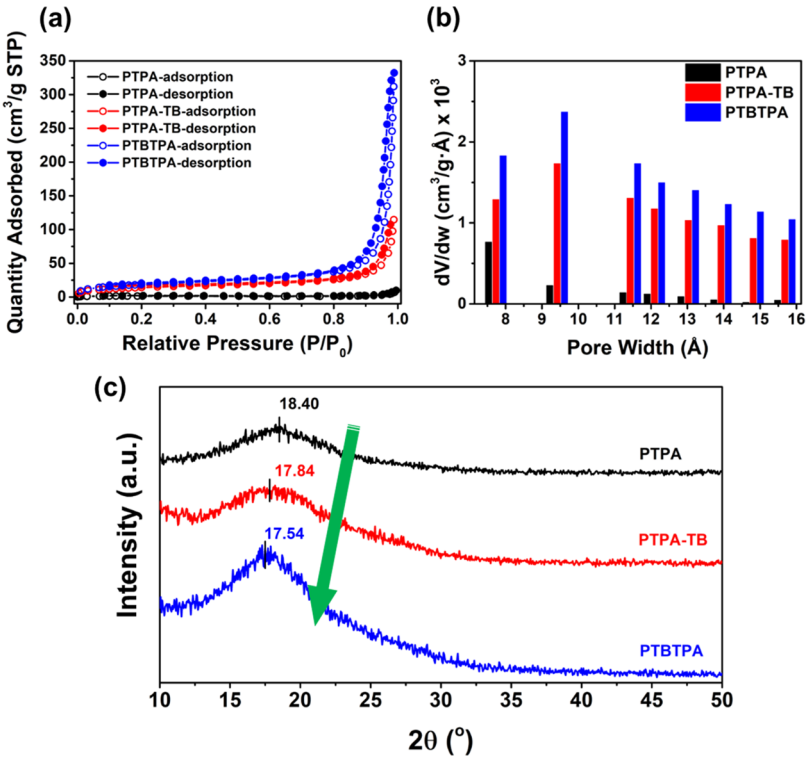

Figure 2. (a) N_2 adsorption and desorption isotherms measured at 77 K. (b) The pore width distribution analyzed by nitrogen adsorption at 77 K via the Horvath−Kawazoe method. (c) WXRD patterns of the polymer films (thickness: 20 ± 5 μm).

same trends as the T_g, where PTPA-TB revealed the highest T_s at 345 °C and PTBTPA exhibited a higher T_s (280 °C) than PTPA (270 °C). The thermal decompositions of the prepared polyamides were investigated using TGA. The semiaromatic polyamides, PTPA and PTBTPA containing alicyclic moieties, displayed similar high thermal stability to the wholly aromatic polyamide, PTPA-TB.

3.2.2. Microporous Properties of Polyamides. To gain insight into the microporous characteristics of these polyamides, measurements including density, BET analysis, and wide-angle X-ray diffraction (WXRD) techniques were employed to evaluate the correlation between their physical properties and molecular structures, which are summarized in Figure 2 and Table 1. The densities of the polyamides were measured by a density meter in 2,2,4-trimethylpentane. With the introduction of the distorted and bulky TB scaffolds, PTBTPA (1.164 g/cm^3) and PTPA-TB (1.171 g/cm^3) revealed lower density than PTPA (1.204 g/cm^3), indicating the higher free volume attributed to the looser packing caused by TB moieties. The specific surface areas of these porous polyamides were determined from the nitrogen adsorption−desorption isotherms at 77 K (Figure 2a). The results revealed that the aid of TB building blocks could significantly enhance the specific surface area of the polyamides, where the specific surface area of PTBTPA (68.32 m^2/g) was almost 13 times larger than that of PTPA (5.18 m^2/g), and the surface area of PTPA-TB (51.83 m^2/g) was 10 times larger than PTPA.

Table 1. Microporous Properties of the Prepared Polyamides

index	ρ^a [g/cm^3]	$S_{BET}{}^b$ [m^2/g]	$2\theta^c$ [deg]	d-spacing^d [Å]
PTPA	1.204	5.18	18.40	4.82
PTPA-TB	1.172	51.83	17.84	4.97
PTBTPA	1.164	68.32	17.54	5.05

^{a}The density of the films was measured in 2,2,4-trimethylpentane. ^{b}Calculated by the results of the N_2 adsorption (filled) and desorption (empty) isotherms measured by BET at 77 K. ^{c}Measured by XRD at the scan range of 2θ from 10 to 50°. ^{d}Calculated from the results of the WXRD curve by applying Bragg's law.

Moreover, the pore width distribution of the micropores of the polyamides could be analyzed via the Horvath−Kawazoe method, as depicted in Figure 2b. As anticipated, the results revealed that PTBTPA and PTPA-TB, which have TB units in the polymer backbones, displayed a higher density of micropores than PTPA. Furthermore, the aggregation behaviors of the polymer chains were investigated by WXRD in Figure 2c. All of the polyamides revealed broad diffraction peaks of the amorphous patterns. PTPA showed a diffraction peak at 18.40°, while PTBTPA and PTPA-TB showed smaller diffraction angles at 17.54 and 17.84°. Bragg's law calculations determined that the d-spacing values for PTPA, PTPA-TB, and PTBTPA were 4.82, 4.97, and 5.05 Å, respectively. The results showed that the presence of rigid and distorted TB building blocks led to the separation and inefficient packing of polymer chains, promoting the creation of micropores. Moreover, the bulky and distorted monomer structure of PTBTPA makes a larger d-spacing than that of PTPA-TB, lowering the density and increasing the specific surface area.

3.3. Electrochemical Properties of Model Compounds. To elucidate the electrochemical behaviors of PTBTPA, a related model compound of TBTPA-M was applied to examine the electrochemical characteristics. In Figure 3a, comparing the first oxidation potential of amide-type model compounds, TBTPA-M and TPA-M, it was found that the oxidation potential reveals a slight decrease after

https://doi.org/10.1021/acsapm.3c02288
ACS Appl. Polym. Mater. 2024, 6, 658−668

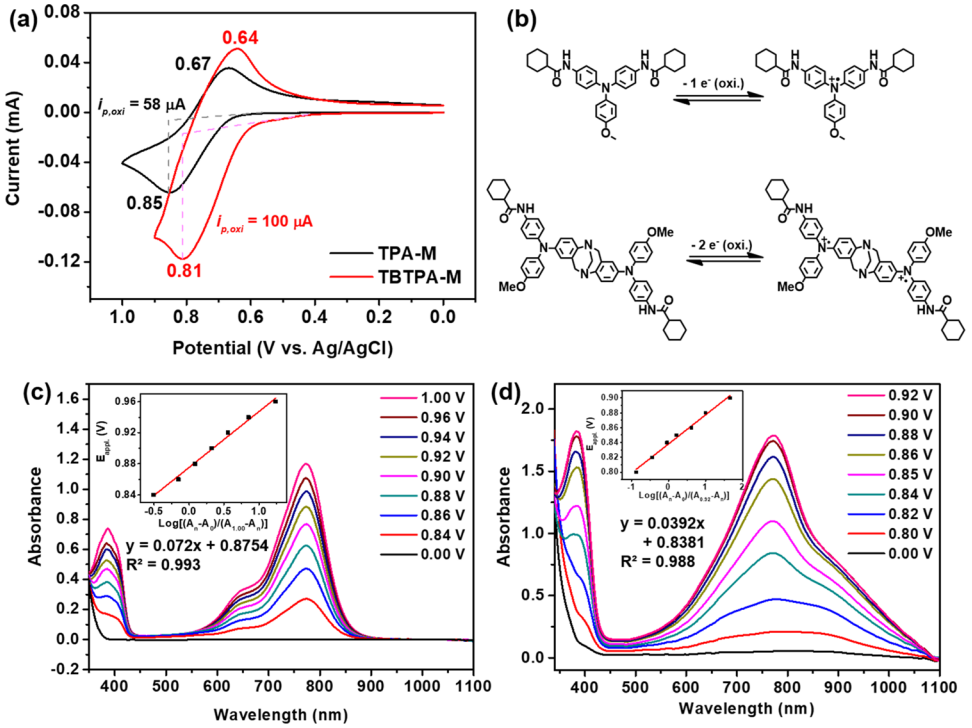

Figure 3. (a) Cyclic voltammetry diagrams of TPA-M and TBTPA-M conducted with platinum net in an optically transparent thin-layer electrode (OTTLE) cell at a scan rate of 50 mV/s (sample amount: 0.5 μmol in 1 mL of 0.1 M TBAP/GBL). (b) The oxidation process of TPA-M and TBTPA-M. (c, d) Spectroelectrochemistry diagrams and Nernstian analysis of (c) TPA-M and (d) TBTPA-M at different applied potentials (the spectral profiles are recorded after 1 min at specified potential; sample amount: 0.5 μmol in 1 mL of 0.1 M TBAP/GBL).

introducing a Tröger's base core to the molecular structure (TPA-M: $E_{oxi.}$ = 0.85 V; TBTPA-M: $E_{oxi.}$ = 0.81 V) because of the electro-donating ability of the TB unit at the center. Furthermore, the peak current of TBTPA-M ($i_{p,oxi.}$ = 100 μA) was almost 2 times greater than that of TPA-M ($i_{p,oxi.}$ = 58 μA) in the same molar concentration, implying that the two electroactive sites of TBTPA-M oxidized simultaneously at the oxidation state. An extensive analysis of spectroelectrochemistry was carried out via the Nernst equation to verify the assumption of a two-electron process in the oxidation of TBTPA-M. The applied potential ($E_{appl.}$) and the number of electrons transferred (n) could be described by the Nernst equation as the following:

$$E_{appl.} = E_0 + \frac{0.0592}{n}\log\left(\frac{[O]}{[N]}\right) \quad (1)$$

where E_0 is the formal oxidation potential and [O] and [N] are the concentrations of the oxidized/neutral species, respectively.

In the dilute solution, the concentration of the neutral/oxidized species was proportional to the absorbance according to Beer's law. Thus, the ratio of the oxidized species to the neutral species could be calculated from the absorbance. Herein, the results of spectroelectrochemical measurements are depicted in Figure 3c,d with the sequential increase of the applied potential. We assume that the potential of the maximum absorbance of each compound was proportional to the mole of the oxidized electroactive species. Therefore, the following equation could present the ratio of the oxidized species to the neutral species:

$$\frac{[O]}{[N]} = \frac{(A_n - A_0)}{(A_{max} - A_n)} \quad (2)$$

where A_n is the absorbance at a specific applied potential and A_0 and A_{max} are the absorbances at the neutral and fully oxidized states. After the applied potentials ($E_{appl.}$, y-axis) were plotted to the logarithms of the concentration ratio (x-axis), the slope of the fitting line could be converted to the number of electrons transferred. For the ideal one-electron and two-electron oxidation, the Nernstian value (slope of the fitting line) should be 59.2 mV and 29.6 mV, respectively. The Nernstian value for TBTPA-M is 39.2 mV, which could be considered the two-electron process. For comparison, the Nernstian value for TPA-M is 72.0 mV for a one-electron process. These results matched our group's previous work,[43] confirming that Tröger's base linkage isolated the two redox sites of the triphenylamine center of TBTPA-M, making it oxidize simultaneously during the first oxidation.

3.4. Electrochemical Properties of Polyamide Films.

The polymeric electrode for electrochemical measurements was prepared by drop-casting the polymer solution on an ITO-coating glass. The thickness of the polyamide films was measured by an α-step profiler and is recorded in Figure S23, and the detailed procedure of sample preparation is described in the Supporting Information. The electrochemical behaviors of the intrinsically porous polyamide films were evaluated by cyclic voltammetry at a scan rate of 50 mV/s in 3 mL of 0.1 M $TBABF_4$/MeCN, as shown in Figure 4a and summarized in Table 2. With the incorporation of TB units, the oxidation potential of PTBTPA ($E_{oxi.}$ = 1.00 V) and PTPA-TB ($E_{oxi.}$ = 1.02 V) was slightly decreased in comparison to PTPA ($E_{oxi.}$ = 1.05 V). Moreover, the potential differences (ΔE) of the TB-incorporated polyamides, PTBTPA (ΔE = 0.39 V) and PTPA-TB (ΔE = 0.46 V), were significantly lower than PTPA (ΔE = 0.57 V), indicating that the microporous properties generated by the rigid and distorted TB units facilitated the diffusion of

https://doi.org/10.1021/acsapm.3c02288
ACS Appl. Polym. Mater. 2024, 6, 658−668

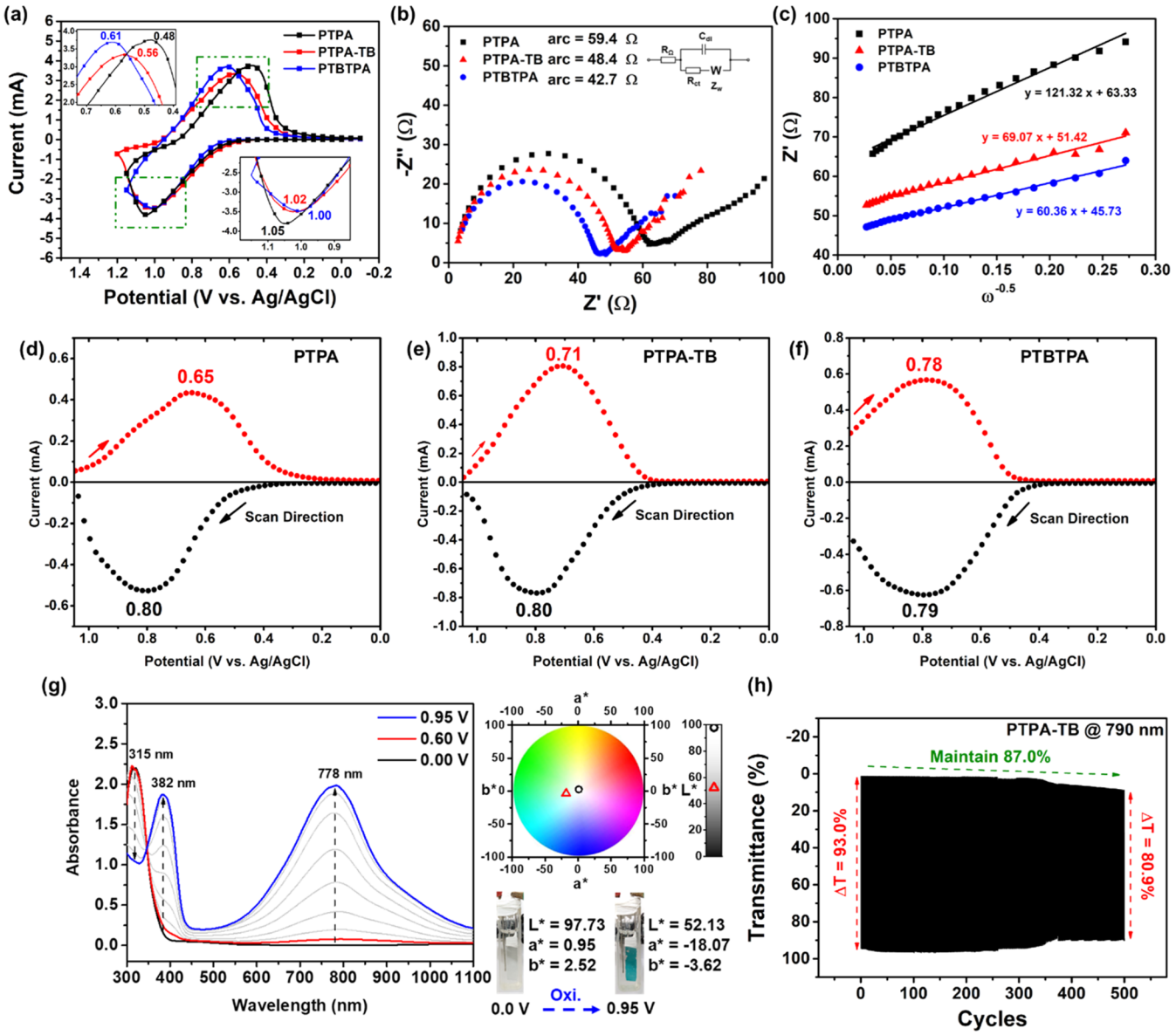

Figure 4. (a) Cyclic voltammetry diagrams of resulting polyamides measured on the ITO-coated glass substrate at a scan rate of 50 mV/s. (b) Nyquist plots of PTPA, PTBTPA, and PTPA-TB and (c) the relationship between Z' and $\omega^{-0.5}$ in the corresponding low-frequency region. Differential pulse voltammetry diagrams of (d) PTPA, (e) PTPA-TB, and (f) PTBTPA measured on ITO-coated glass substrates at an increment of 4 mV, a pulse width of 25 ms, a pulse period of 0.2 s, and a pulse amplitude of 50 mV (black: positive scan, red: negative scan). (g) Spectroelectrochemical spectra and CIELAB color space parameters of the PTBTPA film measured on the ITO-coated glass substrate (the spectral profiles are recorded after 1 min at specified potential). (h) Switching stability of the PTBTPA film between −0.1 and 0.85 V for 500 cycles with a cycle time of 40 s. All of the experiments were conducted on the ITO-coated glass substrate in 3 mL of 0.1 M $TBABF_4$/MeCN in a 360 ± 30 nm thickness.

Table 2. Electrochemical Properties and Impedance Data of the Prepared Polyamide Films

index	$E_{oxi.}$[a] [V]	$E_{red.}$[b] [V]	ΔE_{CV}[c] [V]	ΔE_{DPV}[d] [V]	R_{ct}[e] [Ω]	σ_w[f] [Ω/s$^{0.5}$]	D[g] [10^{-10} cm^2/s]
PTPA (360 ± 30 nm)	1.05	0.48	0.57	0.15	59.4	121.32	1.67
PTPA-TB (360 ± 30 nm)	1.02	0.56	0.46	0.09	48.4	69.07	5.16
PTBTPA (360 ± 30 nm)	1.00	0.61	0.39	0.01	42.7	60.36	6.75

[a]Oxidation peak potential. [b]Reduction peak potential. [c]Potential difference between oxidation and reduction peaks calculated by CV measurement, $|E_{oxi.} - E_{red.}|$. [d]Potential difference between oxidation and reduction peaks calculated by DPV measurement, $|E_{oxi.} - E_{red.}|$. [e]The charge transfer resistance obtained from the diameter of the arc. [f]The Warburg coefficient obtained from the slope for the plot of Z' vs the reciprocal root square of the lower angular frequencies ($\omega^{-0.5}$). [g]Diffusion coefficient of the counterions in the polyamide matrix.

counterions within the polymer matrix and lowered the ion transfer barrier.[44,45] In Figure 4d4–f, the differential pulse voltammetry (DPV) diagrams of the polyamide films revealed almost the same oxidation potential (PTPA: 0.80 V, PTBTPA:0.79 V, PTPA-TB: 0.80 V), while the reduction peaks in the reverse DPV scan showed much difference.

https://doi.org/10.1021/acsapm.3c02288
ACS Appl. Polym. Mater. 2024, 6, 658−668

Table 3. Electrochromic Properties of the Prepared Polyamide Films

index	λ_{onset}[a] [nm]	t_c[b] [s]	t_b[c] [s]	ΔT[d] [%]	υ_c[e] [%/s]	η_{CE}[f] [cm²/C]	stability[g] [%]
PTPA (360 ± 30 nm)	381	5.7	8.6	98.2	15.1	310	82.1
PTPA-TB (360 ± 30 nm)	417	1.8	1.5	93.9	47.0	435	87.0
PTBTPA (360 ± 30 nm)	385	1.8	1.5	97.1	48.6	353	89.0

[a]The absorption onset wavelength is obtained from the spectroelectrochemical spectra at a neutral state (0 V). [b]Coloring time from the bleaching state to 90% of total transmittance change. [c]Bleaching time from the coloring state to 90% of total transmittance change. [d]Change in transmittance is $\Delta T = T_b - T_c$, where T_b and T_c are the transmittances of bleaching and coloring states, respectively. [e]Coloration response speed is defined as 90% of ΔT divided by t_c. [f]Coloration efficiency is determined by the slope of change in optical density (ΔOD) versus charge density. Change in optical density is defined as $\Delta OD = \log [T_b/T_c]$. [g]The remaining change in transmittance after 500 cycles.

PTBTPA demonstrated almost no potential difference between the oxidation and reduction peaks (0.79/0.78 V; ΔE = 0.01 V), implying an accelerated reduction process facilitated by micropore structures. PTPA-TB also revealed a slight potential difference (0.80/0.71 V, ΔE = 0.09 V) when the TB unit was introduced into the polymer backbone. In contrast, PTPA possessed a broad reduction peak with the most significant potential difference (0.80/0.65 V, ΔE = 0.15 V), demonstrating the restriction of the reduction process due to the dense packing of the polymer chain.

To further analyze the electron transfer mechanism of the polyamide films, electrochemical impedance spectroscopy (EIS) was adopted using the Randles circuit as a model to determine the conductivity and resistance of the electroactive polyamides. This model is composed of a solution resistance (R_Ω) in series with a parallel combination of double-layer capacitance (C_{dl}) and a series connection of charge transfer resistance (R_{ct}) and Warburg impedance (Z_W). Figure 4b,c and Table 2 present the Nyquist plots and the fitting parameters of the polyamides. R_{ct} value was determined by measuring the arc length of the semicircles in the Nyquist plots, where PTBTPA (42.7 Ω) and PTPA-TB (48.4 Ω) revealed a lower resistance in comparison to PTPA (59.4 Ω). The lower energy barrier of charge transfer might be attributed to the high charge mobility of the TB core and the high affinity between two electron-rich nitrogen atoms in the TB unit and the ITO surface due to the hydrogen bond interaction.[12,46,47] Furthermore, the diffusion coefficient (D) of the counterions in the polymer matrix was also calculated to evaluate the ion-transport behaviors. As shown in Figure 4c and Table 2, the incorporation of TB scaffolds significantly increased the diffusivity of the counterions, BF_4^-, where the diffusion coefficients of BF_4^- increased to 3−4 times higher in PTBTPA (6.75×10^{-10} cm²/s) and PTPA-TB (5.16×10^{-10} cm²/s) in comparison to PTPA (1.67×10^{-10} cm²/s). The observed correlation between the diffusivity of counterions and the microporosity of the polymer suggests a potential avenue for designing and developing polymeric devices with enhanced response capabilities.

3.5. EC Properties of Polyamide Films. Spectroelectrochemical measurements were carried out to evaluate the electrochromic properties of these intrinsically porous polyamide films. In Figures 4g, S24 and S25, all of these polyamides possessed high transparency in the neutral state, showing high L^* values. The onset wavelength (λ_{onset}) of PTPA and PTBTPA at the neutral state showed approximately 20 nm shorter than PTPA-TB owing to the alicyclic moiety causing less charge transfer in the polymer backbone to result in a colorless feature at the neutral state, showing that PTPA and PTBTPA manifested much smaller b^* than PTPA-TB, as tabulated in Table 3. These polyamides displayed their characteristic absorption peaks around 385 and 780 nm as the applied potential was increased to 0.95 V, and the appearance of the polymer films turned into dense teal and green colors. The switching response characteristics of the polyamide films were 0.95 V as the coloring voltage and −0.1 V as the bleaching voltage for 20 s each. As shown in Figure S26 and Table 3, PTPA required 5.7 s for coloring and 8.6 s for bleaching to reach 90% of the total optical difference in transmittance. For comparison, incorporating TB scaffolds into polyamides had a notable impact on the response times with shorter times observed for coloring and bleaching. PTBTPA and PTPA-TB showed a response time of 1.8 s for coloring and 1.5 s for bleaching, 68 and 83% shorter than PTPA. These three polyamides revealed a high change in transmittance of over 93%, and PTBTPA could perform the highest optical difference at 97.1%. Therefore, the calculated coloration response speed was 15.1, 47.0, and 48.6% s^{-1} for PTPA, PTPA-TB, and PTBTPA, respectively. The coloration response capability could be enhanced significantly due to the generation of micropores in the polyamides.

For the current consumption of the polyamide films (Figure S27), the TB-incorporated polyamides, PTBTPA and PTPA-TB, demonstrated sharper current peaks and less charge consumption during both the coloring and bleaching processes, indicating the more efficient redox process. In other words, the lower charge consumption could cause higher coloration efficiency, showing 353 and 435 cm²/C for PTBTPA and PTPA-TB, compared to PTPA (310 cm²/C), as shown in Figure S28. Moreover, the switching stability of the polyamide films is illustrated and summarized in Figures 4h and S29 and Table 3, respectively. With the more excellent response capability, PTBTPA and PTPA-TB showed higher stability (89.0 and 87.0%) after 500 cycles, while the poor bleaching capability of PTPA resulted in color retention in the bleaching state over 100 cycles.

3.6. EC Behaviors of the Corresponding ECDs. To estimate the practical EC application, the gel-type EC devices (ECDs) were fabricated with the combination of heptyl viologen (HV) as the complementary EC material, which could enhance the EC properties of the devices. The description of the detailed procedures is summarized and depicted in the Supporting Information and Figure S30. The CV and DPV diagrams of the ECDs are depicted in Figures S31 and S32, where PTPA/HV showed the oxidation potential at 1.24 V and reduction potential at 1.01 V. In comparison, the TB-incorporated ECDs, PTBTPA/HV and PTPA-TB/HV, displayed a redox potential at 1.12/0.99 and 1.19/1.02 V, respectively, following the same tendency as polymer films. Interestingly, PTBTPA exhibited the lowest applied voltage for on-state within the prepared devices and nearly zero value in ΔE in the DPV measurement, contributing to the aid of the TB core between two TPA moieties. The spectroelectrochemistry

https://doi.org/10.1021/acsapm.3c02288
ACS Appl. Polym. Mater. 2024, 6, 658−668

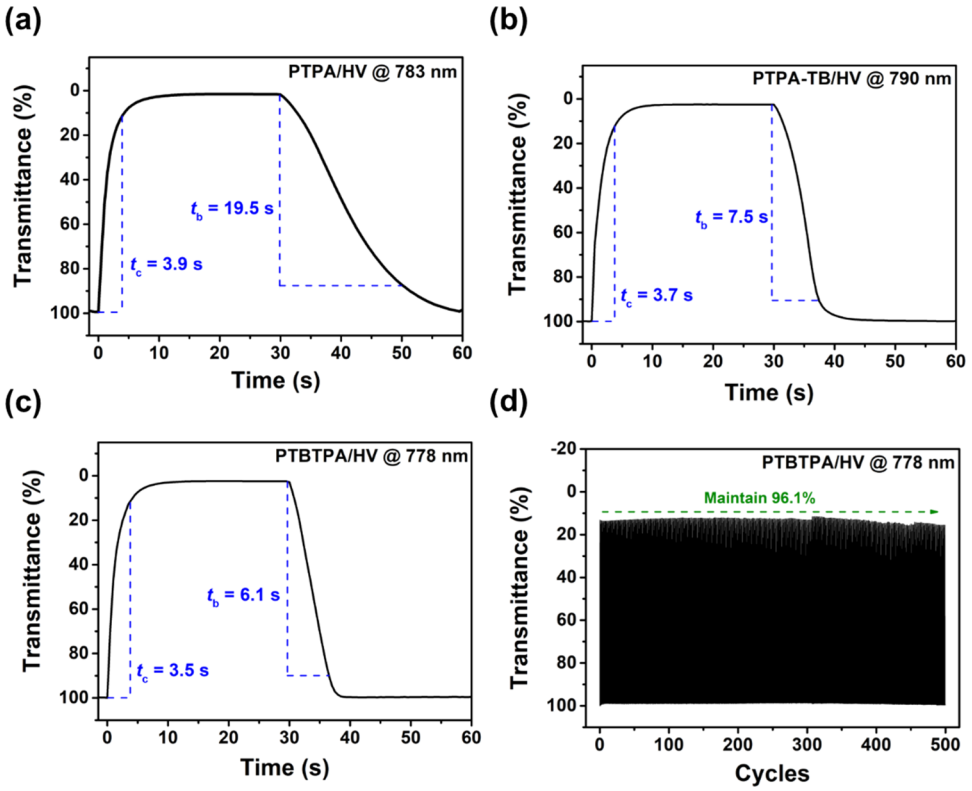

Figure 5. Response time of (a) PTPA/HV, (b) PTBTPA/HV, (c) PTPA-TB/HV ECDs between −0.3 and 1.25 V with a cycle time of 60 s, and (d) switching stability of PTBTPA/HV between −0.1 and 1.25 V for 500 cycles with a cycle time of 60 s.

diagrams and the corresponding parameters of the CIELAB color space are shown in Figures S33−S35, as the incorporation of HV, a new absorption band generated around 608 nm, complements a part of the optical window of the TPA cation radical. The TB-incorporated ECDs, PTBTPA/HV and PTPA-TB/HV, demonstrated their coloring time and bleaching time for 3.5/6.1 and 3.7/7.5 s, respectively, which were shorter than PTPA/HV (3.9/19.5 s), as illustrated and summarized in Figure 5a−5c and Table 4. The most minor ejected charge of PTBTPA/HV resulted in the highest coloration efficiency (337 cm^2/C) and the highest stability, keeping 96.1% of the ΔT after 500 continuous switching cycles among the devices, as illustrated in Figures 5d and S36−S38.

Table 4. Electrochromic Parameters of ECDs

index	t_c[a] [s]	t_b[b] [s]	ΔT[c] [%]	v_c[d] [%/s]	η_{CE}[e] [cm^2/C]	stability[f] [%]
PTPA/HV	3.9	19.5	98.1	22.6	284	90.3
PTPA-TB/HV	3.7	7.5	97.0	23.6	305	94.2
PTBTPA/HV	3.5	6.1	97.5	25.1	337	96.1

[a]Coloring time from the bleaching state to 90% of total transmittance change. [b]Bleaching time from the coloring state to 90% of total transmittance change. [c]Change in transmittance is $\Delta T = T_b - T_c$, where T_b and T_c are the transmittances of bleaching and coloring states, respectively. [d]Coloration response speed is defined as 90% of ΔT divided by t_c. [e]Coloration efficiency is determined by the slope of change in optical density (ΔOD) versus charge density. Change in optical density is defined as $\Delta OD = \log[T_b/T_c]$. [f]The remaining change in transmittance after 500 cycles.

4. CONCLUSIONS

A well-designed redox-active TB-incorporated arylamine monomer, TBTPA-NH_2, was successfully synthesized. The TB unit separates two electroactive centers that can oxidize simultaneously at the oxidation state, proven by TBTPA-M through the Nernstian analysis. The polyamide derived from TBTPA-NH_2 revealed the lowest density (1.164 g/cm^3), highest specific surface area (68.32 m^2/g), and largest *d*-spacing (5.05), which can be attributed to the unique V-shaped TB building block to facilitate the inefficient packing of polymer chains. For the electrochemical behaviors of the TB-incorporated polyamides, the micropores significantly increased the diffusion rate of the counterions in the polymer matrix, yielding smaller ΔE (ΔE_{DPV} = 0.01 V), accelerating the response speed (v_c = 48.6% $^{-1}$), enhancing the coloration efficiency (η_{CE} = 353 cm^2/C), and showing remarkable switching stability. Furthermore, the fabricated ECD, PTBTPA/HV, exhibits the best response capability, highest coloration efficiency (η_{CE} = 337 cm^2/C), and remarkable switching stability (96.1% after 500 cycles of switching) for practical applications. This study demonstrates the potential of incorporating bulky TB units into polyamides to generate micropores as a design strategy for preparing high-performance electrochromic materials, paving the way for developing more energy-efficient and superior devices.

■ ASSOCIATED CONTENT

Supporting Information

The Supporting Information is available free of charge at https://pubs.acs.org/doi/10.1021/acsapm.3c02288.

Synthesis of model compounds; preparation of the polymer films and the detailed measurement informa-

https://doi.org/10.1021/acsapm.3c02288
ACS Appl. Polym. Mater. 2024, 6, 658−668

tion; FTIR spectra, ^{1}H and ^{13}C NMR spectra, and mass spectra of the prepared monomers and polymers, thermal properties and spectroelectrochemical diagrams of the prepared polymer films (PDF)

AUTHOR INFORMATION

Corresponding Authors

Chien-Chieh Hu − *Graduate Institute of Applied Science and Technology, National Taiwan University of Science and Technology, Taipei 106335, Taiwan;* orcid.org/0000-0002-3379-1764; Email: cchu@mail.ntust.edu.tw

Guey-Sheng Liou − *Institute of Polymer Science and Engineering, National Taiwan University, Taipei 10617, Taiwan;* orcid.org/0000-0003-3725-3768; Email: gsliou@ntu.edu.tw

Authors

Min-Hsiu Tu − *Institute of Polymer Science and Engineering, National Taiwan University, Taipei 10617, Taiwan*

Yu-Jen Shao − *Institute of Polymer Science and Engineering, National Taiwan University, Taipei 10617, Taiwan*

Hou-Lin Li − *Institute of Polymer Science and Engineering, National Taiwan University, Taipei 10617, Taiwan*

Complete contact information is available at: https://pubs.acs.org/10.1021/acsapm.3c02288

Author Contributions

[§]M.-H. Tu, Y.-J. Shao, and H.-L. Li contributed equally.

Notes

The authors declare no competing financial interest.

ACKNOWLEDGMENTS

This work received financial support from the National Science and Technology Council in Taiwan (NSTC, 111-2113-M-002-024 and 111-2221-E-002-028-MY3). The authors gratefully thank Chiu-Hui He in the Instrumentation Center at NTNU for assistance in NMR measurements, Chia-Bin Hung in the Precious Instrumentation Center at NTUST for assistance in XRD measurements, and the Instrumentation Center at NTU for HRMS measurements.

REFERENCES

(1) Gu, C.; Jia, A. B.; Zhang, Y. M.; Zhang, S. X. A. Emerging electrochromic materials and devices for future displays. *Chem. Rev.* **2022**, *122* (18), 14679−14721.

(2) Rai, V.; Singh, R. S.; Blackwood, D. J.; Zhili, D. A review on recent advances in electrochromic devices: a material approach. *Adv. Eng. Mater.* **2020**, *22* (8), No. 2000082.

(3) Zhai, Y.; Li, J.; Shen, S.; Zhu, Z.; Mao, S.; Xiao, X.; Zhu, C.; Tang, J.; Lu, X.; Chen, J. Recent Advances on Dual-Band Electrochromic Materials and Devices. *Adv. Funct. Mater.* **2022**, *32* (17), No. 2109848.

(4) Krebs, F. C. The new black. *Nat. Mater.* **2008**, *7* (10), 766−767.

(5) Beaujuge, P. M.; Ellinger, S.; Reynolds, J. R. The donor−acceptor approach allows a black-to-transmissive switching polymeric electrochrome. *Nat. Mater.* **2008**, *7* (10), 795−799.

(6) Li, T.; Li, S.; Li, X.; Xu, Z.; Zhao, J.; Shi, Y.; Wang, Y.; Yu, R.; Liu, X.; Xu, Q.; Guo, W. A leaf vein-like hierarchical silver grids transparent electrode towards high-performance flexible electrochromic smart windows. *Sci. Bull.* **2020**, *65* (3), 225−232.

(7) Baetens, R.; Jelle, B. P.; Gustavsen, A. Properties, requirements and possibilities of smart windows for dynamic daylight and solar energy control in buildings: A state-of-the-art review. *Sol. Energy Mater. Sol. Cells* **2010**, *94* (2), 87−105.

(8) Yu, H.; Shao, S.; Yan, L.; Meng, H.; He, Y.; Yao, C.; Xu, P.; Zhang, X.; Hu, W.; Huang, W. Side-chain engineering of green color electrochromic polymer materials: toward adaptive camouflage application. *J. Mater. Chem. C* **2016**, *4* (12), 2269−2273.

(9) Wei, D.; Scherer, M. R. J.; Bower, C.; Andrew, P.; Ryhänen, T.; Steiner, U. A Nanostructured Electrochromic Supercapacitor. *Nano Lett.* **2012**, *12* (4), 1857−1862.

(10) Zhang, W.; Li, H.; Al Hussein, M.; Elezzabi, A. Y. Electrochromic Battery Displays with Energy Retrieval Functions Using Solution-Processable Colloidal Vanadium Oxide Nanoparticles. *Adv. Opt. Mater.* **2020**, *8* (2), No. 1901224.

(11) Yun, T. G.; Chen, X.; Cheong, J. Y. Research in Electrochromic Supercapacitor−A Focused Review. *Batteries Supercaps* **2023**, *6* (3), No. e202200454.

(12) Shao, Y.-J.; Yen, T. C.; Hu, C. C.; Liou, G. S. Non-Conjugated Triarylamine-Based Intrinsic Microporous Polyamides for Electrochromic Supercapacitor: Diffusion Dynamics and Charge-Discharge Studies. *J. Mater. Chem. A* **2023**, *11*, 1877−1885.

(13) Chang, C. W.; Liou, G. S.; Hsiao, S. H. Highly stable anodic green electrochromic aromatic polyamides: synthesis and electrochromic properties. *J. Mater. Chem.* **2007**, *17* (10), 1007−1015.

(14) Liou, G. S.; Chang, C. W. Highly Stable Anodic Electrochromic Aromatic Polyamides Containing N,N,N′,N′-Tetraphenyl-p-Phenylenediamine Moieties: Synthesis, Electrochemical, and Electrochromic Properties. *Macromolecules* **2008**, *41* (5), 1667−1674.

(15) Yen, H. J.; Lin, H. Y.; Liou, G. S. Novel Starburst Triarylamine-Containing Electroactive Aramids with Highly Stable Electrochromism in Near-Infrared and Visible Light Regions. *Chem. Mater.* **2011**, *23* (7), 1874−1882.

(16) Yen, H. J.; Liou, G. S. Design and preparation of triphenylamine-based polymeric materials towards emergent optoelectronic applications. *Prog. Polym. Sci.* **2019**, *89*, 250−287.

(17) Shao, Y. J.; Tu, M. H.; Liou, G. S. Unprecedented facile approach of multiple amino-substituted triphenylamine derivatives for electrochromic devices with extremely high coloration efficiency and unexpected redox stability. *Chem. Eng. J.* **2023**, *466*, No. 143003.

(18) Liu, H. S.; Pan, B. C.; Huang, D. C.; Kung, Y. R.; Leu, C. M.; Liou, G. S. Highly transparent to truly black electrochromic devices based on an ambipolar system of polyamides and viologen. *NPG Asia Mater.* **2017**, *9* (6), e388.

(19) Chiu, Y. W.; Tan, W. S.; Yang, J. S.; Pai, M. H.; Liou, G. S. Electrochromic Response Capability Enhancement with Pentiptycene-Incorporated Intrinsic Porous Polyamide Films. *Macromol. Rapid Commun.* **2020**, *41* (12), No. 2000186.

(20) Pai, M. H.; Hu, C. C.; Liou, G. S. Enhancement of Electrochromic Switching Properties with Tröger's Base-Derived Intrinsic Microporous Polyamide Films. *Macromol. Rapid Commun.* **2021**, *42* (23), No. 2100492.

(21) Pai, M. H.; Hu, C. C.; Tan, W. S.; Yang, J. S.; Liou, G. S. Preparation and Characterization of Intrinsic Porous Polyamides Based on Redox-Active Aromatic Diamines with Pentiptycene Scaffolds. *ACS Macro Lett.* **2021**, *10* (10), 1210−1215.

(22) Shamsabadi, A. A.; Rezakazemi, M.; Seidi, F.; Riazi, H.; Aminabhavi, T.; Soroush, M. Next generation polymers of intrinsic microporosity with tunable moieties for ultrahigh permeation and precise molecular CO2 separation. *Prog. Energy Combust. Sci.* **2021**, *84*, No. 100903.

(23) Wang, L.; Zhao, Y.; Fan, B.; Carta, M.; Malpass-Evans, R.; McKeown, N. B.; Marken, F. Polymer of intrinsic microporosity (PIM) films and membranes in electrochemical energy storage and conversion: A mini-review. *Electrochem. Commun.* **2020**, *118*, No. 106798.

(24) Lee, W. H.; Seong, J. G.; Hu, X.; Lee, Y. M. Recent progress in microporous polymers from thermally rearranged polymers and polymers of intrinsic microporosity for membrane gas separation: pushing performance limits and revisiting trade-off lines. *J. Polym. Sci.* **2020**, *58* (18), 2450−2466.

(25) Wang, Y.; Ghanem, B. S.; Ali, Z.; Hazazi, K.; Han, Y.; Pinnau, I. Recent progress on polymers of intrinsic microporosity and thermally

modified analogue materials for membrane-based fluid separations. *Small Struct.* **2021**, *2* (9), No. 2100049.
(26) McKeown, N. B. The structure-property relationships of Polymers of Intrinsic Microporosity (PIMs). *Curr. Opin. Chem. Eng.* **2022**, *36*, No. 100785.
(27) Emmler, T.; Heinrich, K.; Fritsch, D.; Budd, P. M.; Chaukura, N.; Ehlers, D.; Rätzke, K.; Faupel, F. Free Volume Investigation of Polymers of Intrinsic Microporosity (PIMs): PIM-1 and PIM1 Copolymers Incorporating Ethanoanthracene Units. *Macromolecules* **2010**, *43* (14), 6075−6084.
(28) Ghanem, B. S.; Msayib, K. J.; McKeown, N. B.; Harris, K. D. M.; Pan, Z.; Budd, P. M.; Butler, A.; Selbie, J.; Book, D.; Walton, A. A triptycene-based polymer of intrinsic microposity that displays enhanced surface area and hydrogen adsorption. *Chem. Commun.* **2007**, No. 1, 67−69.
(29) Weidman, J. R.; Guo, R. The Use of Iptycenes in Rational Macromolecular Design for Gas Separation Membrane Applications. *Ind. Eng. Chem. Res.* **2017**, *56* (15), 4220−4236.
(30) Weber, J.; Thomas, A. Toward Stable Interfaces in Conjugated Polymers: Microporous Poly(p-phenylene) and Poly(phenyleneethynylene) Based on a Spirobifluorene Building Block. *J. Am. Chem. Soc.* **2008**, *130* (20), 6334−6335.
(31) Bezzu, C. G.; Carta, M.; Tonkins, A.; Jansen, J. C.; Bernardo, P.; Bazzarelli, F.; McKeown, N. B. A Spirobifluorene-Based Polymer of Intrinsic Microporosity with Improved Performance for Gas Separation. *Adv. Mater.* **2012**, *24* (44), 5930−5933.
(32) Carta, M.; Evans, R. M.; Croad, M.; Rogan, Y.; Jansen, J. C.; Bernardo, P.; Bazzarelli, F.; McKeown, N. B. An Efficient Polymer Molecular Sieve for Membrane Gas Separations. *Science* **2013**, *339* (6117), 303−307.
(33) Lee, M.; Bezzu, C. G.; Carta, M.; Bernardo, P.; Clarizia, G.; Jansen, J. C.; McKeown, N. B. Enhancing the Gas Permeability of Tröger's Base Derived Polyimides of Intrinsic Microporosity. *Macromolecules* **2016**, *49* (11), 4147−4154.
(34) McKeown, N. B. Polymers of Intrinsic Microporosity. *ISRN Mater. Sci.* **2012**, *2012*, No. 513986.
(35) Tröger, J. Ueber einige mittelst nascirenden Formaldehydes entstehende Basen. *J. Prakt. Chem.* **1887**, *36* (1), 225−245.
(36) Neogi, I.; Jhulki, S.; Ghosh, A.; Chow, T. J.; Moorthy, J. N. Amorphous Host Materials Based on Tröger's Base Scaffold for Application in Phosphorescent Organic Light-Emitting Diodes. *ACS Appl. Mater. Interfaces* **2015**, *7* (5), 3298−3305.
(37) Braukyla, T.; Xia, R.; Daskeviciene, M.; Malinauskas, T.; Gruodis, A.; Jankauskas, V.; Fei, Z.; Momblona, C.; Roldán Carmona, C.; Dyson, P. J.; Getautis, V.; Nazeeruddin, M. K. Inexpensive Hole-Transporting Materials Derived from Tröger's Base Afford Efficient and Stable Perovskite Solar Cells. *Angew. Chem., Int. Ed.* **2019**, *58* (33), 11266−11272.
(38) Braukyla, T.; Xia, R.; Malinauskas, T.; Daskeviciene, M.; Magomedov, A.; Kamarauskas, E.; Jankauskas, V.; Fei, Z.; Roldán Carmona, C.; Momblona, C.; Nazeeruddin, M. K.; Dyson, P. J.; Getautis, V. Application of a Tetra-TPD-Type Hole-Transporting Material Fused by a Tröger's Base Core in Perovskite Solar Cells. *Sol. RRL* **2019**, *3* (9), No. 1900224.
(39) Zhuang, Y.; Orita, R.; Fujiwara, E.; Zhang, Y.; Ando, S. Colorless Partially Alicyclic Polyimides Based on Tröger's Base Exhibiting Good Solubility and Dual Fluorescence/Phosphorescence Emission. *Macromolecules* **2019**, *52* (10), 3813−3824.
(40) Jensen, J. K.; Wärnmark, K. Synthesis of Halogen Substituted Analogues of Tröge' s Base. *Synthesis* **2001**, *2001* (12), 1873−1877.
(41) Liou, G. S.; Lin, H. Y. Synthesis and Electrochemical Properties of Novel Aromatic Poly(amine−amide)s with Anodically Highly Stable Yellow and Blue Electrochromic Behaviors. *Macromolecules* **2009**, *42* (1), 125−134.
(42) Wu, Z.; Jin, J. Synthesis and characterization of novel Tröger's base containing polymers from commercial available diamines. *Macromol. Res.* **2017**, *25* (6), 546−551.
(43) Yen, H. J.; Guo, S. M.; Liou, G. S.; Chung, J. C.; Liu, Y. C.; Lu, Y. F.; Zeng, Y. Z. Mixed-valence class I transition and electrochemistry of bis(triphenylamine)-based aramids containing isolated ether-linkage. *J. Polym. Sci., Part A: Polym. Chem.* **2011**, *49* (17), 3805−3816.
(44) Lv, X.; Yan, S.; Dai, Y.; Ouyang, M.; Yang, Y.; Yu, P.; Zhang, C. Ion diffusion and electrochromic performance of poly(4,4′,4″-tris[4-(2-bithienyl)phenyl]amine) based on ionic liquid as electrolyte. *Electrochim. Acta* **2015**, *186*, 85−94.
(45) Cho, S. I.; Lee, S. B. Fast electrochemistry of conductive polymer nanotubes: synthesis, mechanism, and application. *Acc. Chem. Res.* **2008**, *41* (6), 699−707.
(46) Braukyla, T.; Sakai, N.; Daskeviciene, M.; Jankauskas, V.; Kamarauskas, E.; Malinauskas, T.; Snaith, H. J.; Getautis, V. Synthesis and Investigation of the V-shaped Tröger's Base Derivatives as Hole-transporting Materials. *Chem. − Asian J.* **2016**, *11* (14), 2049−2056.
(47) Chen, X.; Zhang, Z.; Wu, L.; Fan, Y.; Tang, H.; Li, N. Hydrogen bonding-induced 6FDA-DABA/TB polymer blends for high performance gas separation membranes. *J. Membr. Sci.* **2022**, *655*, No. 120575.

https://doi.org/10.1021/acsapm.3c02288
ACS Appl. Polym. Mater. 2024, 6, 658−668